ISSN (Print) 1226-1750
ISSN (Online) 2233-6656
Journal of Magnetics 26(3), 322-331 (2021) https://doi.org/10.4283/JMAG.2021.26.3.322

Synthesis and Characterization of FeNi-based Composite Powder from the Mixture of Fe-based Amorphous Powders and Crystalline Ni powders

Jinyoung Kim, Jiyong Hwang, and Seonghoon Yi*

Department of Materials Science and Metallurgical Engineering, Kyungpook National University, Daegu 41566, Republic of Korea

(Received 21 June 2021, Received in final form 29 July 2021, Accepted 5 August 2021)

Fe–Ni alloys have attracted interest as important magnetic alloys without rare-earth (RE) elements, which exhibit a wide variety of magnetic properties depending on the atomic ratios of Fe and Ni. Here, we attempted to synthesize Fe-Ni magnetic materials using a Fe based amorphous alloy precursor that is thermodynamically metastable and has more open atomic packing structure than crystalline alloys. High energy ball milling was applied to promote the formation of various Fe-Ni phases using mixtures of the amorphous precursor powder and 10-50% crystalline Ni powder. The as-milled composite powders as well as the composite powders annealed at 673 K were analyzed by X-ray diffractometer, differential scanning calorimeter, scanning electron microscope, and vibrating sample magnetometer to investigate their magnetic properties in terms of phase transformation behavior of the composite powders.

Keywords : FeNi-based composites, mechanical alloying, amorphous alloy, phase transformation, magnetic property

1. Introduction

Fe–Ni alloys with some structures have attracted interest as an important alloy system without rare-earth (RE) elements. They are classified into two categories (permalloys and Invar alloys) according to the atomic ratios of Fe and Ni. Permalloys contain 50-80 at.% Ni and Invar alloys contain 30-40 at.% Ni [1, 2].

Permalloy belongs to a technologically important class of alloy systems owing to its soft magnetic properties [3-6]. Permalloy having the composition $Fe_{19}Ni_{81}$ is the best-known material for passive magnetic shields due to its high magnetic permeability, which concentrates magnetic field lines inside the material and, therefore, rarefied them in ambient space. It has wide applications in medical magnetic resonance imaging and navigational fluxgate sensor. Invar ($Fe_{64}Ni_{36}$) alloys exhibit little thermal expansion due to compensation for the contracting magneto volume effect with thermal expansion. Therefore, they are ideal materials for high-precision instruments, especially for measuring length scales.

Simultaneously, the chemically ordered $L1_0$-type FeNi alloy is a steady star as an alternative for rare-earth magnetic materials with excellent permanent magnetic properties, such as high coercivity (500-4000 Oe) and magnetic anisotropy (1.3×10^7 erg/cm^3) [7-11]. However, due to the extremely sluggish atomic Fe and Ni diffusion below the $L1_0$ order/disorder transition temperature of 593 K, artificial $L1_0$ FeNi magnets have not been fabricated using conventional metallurgical methods [12]. Although Ni diffusion takes 4.6 billion years to completely transform from the disordered γ_1-phase to the $L1_0$ FeNi phase, neutron irradiation at high temperatures [13] and alternate monatomic layer deposition using molecular beam epitaxy [3-6, 14] have been investigated for synthesizing $L1_0$ FeNi. There has been an increasing interest in some ideal approaches for industrial-scale applications and large-scale production. Hence, many studies have investigated possible reproducible methods. To enhance atomic diffusivity below the $L1_0$ transition temperature, some effects of chemical disordered–ordered phase transition of ferromagnetic compounds within the Fe–Ni binary system have been investigated. In particular, rapid solidification techniques have been employed to produce amorphous precursors, followed by annealing to enhance the atomic migration to increase the diffusion rate [15]. In this process, high diffusivity can be obtained at the crystallization of the as-quenched amorphous phase. Recently, the $L1_0$ FeNi phase with high magnetization was achieved in Makino *et al.* [15] by the crystallization

*Corresponding author: Tel: +82-53-950-5561
Fax: +82-53-950-6559, e-mail: yish@knu.ac.kr

of the amorphous phase, followed by annealing. Geng *et al.* [16] reported that a high-energy ball milling process can intensely influence defect structures, and an increase in vacancy and defect contents enhances atomic diffusivity at low temperatures [17]. However, it is unclear whether mechanical milling creates vacancies or structural disorder in an amorphous Fe–Ni system, but both could increase diffusion rates due to the formation of nanocrystals, resulting in either $L1_0$ ordering or the formation of new FeNi compounds after additional heat treatment.

To improve advanced magnetic materials consisting of sustainable and accessible elements, there is a need to approach various advanced techniques to ramp up the new industrial revolution's contribution worldwide. Thus, herein, we synthesized artificial $L1_0$ FeNi alloys using a high-energy ball mill to prepare high-internal-energy precursors having various Ni contents by mechanical deformation.

Herein, mixtures of Fe-based metallic glassy powder with Ni powder were mechanically milled to produce FeNi-based composite precursors containing several hundred nanoscaled Ni phases, which could be transformed into the Fe–Ni compounds at low temperatures. To confirm the effects of Ni content on the phase transformation and magnetic properties, Fe-based composite powders with 10, 20, 30, 40, and 50 wt.% Ni were prepared as precursors. The composite powders were annealed in a tube furnace, and phase transition and magnetic behavior were studied during mechanical alloying and low-temperature annealing.

2. Material and Methods

A master $Fe_{78}Si_9B_{13}$ (at.%) ingot of nominal compositions was prepared by arc melting high-purity elemental constituents (electron-beam melted Fe 99.999 %, Si 99.9 %, and B 99.9 %) under an Ar gas atmosphere. The button was prepared by arc melting five times for guaranteed homogeneity of the master alloy. Amorphous Fe–Si–B ribbons with a width of 1 mm and thickness of approximately 20 μm were prepared by single-roller melt spinning. The amorphous Fe–Si–B powders were prepared by cryogenic milling of amorphous Fe–Si–B ribbons. Following the crushing of the ribbon, flake particles were first screened below 106 μm and further screened for different particle size fractions. The size of the crushed glass powders used in this study is $d < 63$ μm (d is the diameter of the powder particles).

The composite powder was prepared using a ball milling system, Pulverisette 6 (FRITSCH GmbH), operated in the planetary rotation mode with a hardened steel jar. The starting material with various weight ratios (from 10 to 50 wt.%) of amorphous $Fe_{78}Si_9B_{13}$ powder to commercial Ni powder (Alfa Products; purity, 99.99 %; 400 mesh) was used. The starting material for the milling experiments (typically 30 g) was charged into the milling vials equipped with a PTFE O-ring and 10-mm-diameter hardened steel balls with a ball-to-powder mass ratio of about 10:1. The starting materials and the milled products were kept in an ambient atmosphere. The milling time was 50 h, and the rotation speed was 200 rpm. Milling runs were halted for 15 min every 15 min, with a reversal in the rotation direction after each interval to maintain a homogeneous reaction. To minimize possible atmosphere contamination during milling, vial charging and any subsequent sample handling were performed in a Korea glove box under a purified argon atmosphere (less than 1 ppm O_2 and H_2O). No process controlling agent was used. Then, the milled composite powders were sealed in a quartz tube, which was repeatedly evacuated/backfilled with Ar gas to avoid oxidization. Other related case studies were considered to find the optimized parameters for heat treatment, and the heat treatment was conducted at 673 K for 240 h in a tube furnace, followed by slow cooling in air.

The thermal properties were analyzed using a differential scanning calorimeter (DSC, PYRIS Diamond, Perkin Elmer, USA) at a heating rate of 40 K/min. The structural and phase analyses of the milled and heat-treated powders were conducted using an X-ray diffractometer (XRD, D/Max-2500, Rigaku, Japan) with CuKα radiation (λ = 1.54056 Å). Morphological and microstructural characterization of the materials was performed using a field-emission scanning electron microscope (FE-SEM, SU8220, Hitachi, Japan) equipped with an energy-dispersive X-ray spectroscope (EDS) and scanning electron microscope (SEM, Phenom ProX, Nanoscience Instruments, USA). The magnetic properties of the composite powders before and after heat treatment were analyzed at room temperature using a vibrating sample magnetometer (VSM, Model 7404, Lake Shore, United States). A magnetic field of 15,000 Oe was applied after calibration via the measurement of standard Ni and Fe powder at ambient temperature. The hysteresis curves were measured more than twice for the corresponding sample.

3. Results and Discussion

The SEM micrographs of the Ni and $Fe_{78}Si_9B_{13}$ powders are shown in Figs. 1(a) and (b). Fig. 1(b) shows pulverized $Fe_{78}Si_9B_{13}$ ribbons in the shape of irregular thin flakes with a diameter less than 63 μm, whereas the

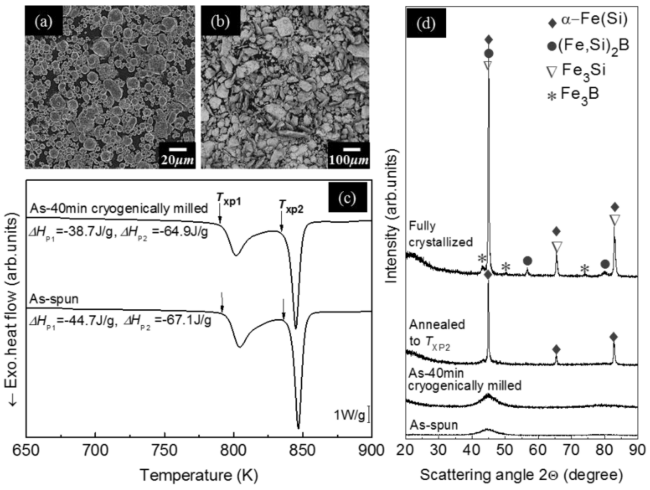

Fig. 1. Morphology of (a) Ni powders and (b) pulverized $Fe_{78}Si_9B_{13}$ particles. (c) DSC curves (40 K/min) and (d) XRD patterns of as-spun cryogenic milled $Fe_{78}Si_9B_{13}$, Txp_2-annealed, and fully crystallized samples.

Ni powder exhibited a spherical shape with a diameter less than 37 μm (Fig. 1(a)).

The isochronal DSC (40 K/min) scans of the as-spun $Fe_{78}Si_9B_{13}$ ribbons and 40-min cryogenically milled $Fe_{78}Si_9B_{13}$ powders are shown in Fig. 1(c). The DSC curves of the $Fe_{78}Si_9B_{13}$ ribbons show typical characteristic features of two separated exothermic peaks, and it indicates that the transformation from the amorphous to the crystalline state proceeded in two main stages. The first crystallization of the as-spun started at 789 K with the enthalpy of crystallization related to the exothermic DSC peak of ΔH_{P1} = 44.7 J/g and induced the formation of primary α-Fe(Si) phase, corresponding to XRD trace of 789 K (Tx_{P2}) annealed samples (Fig. 1(d)). The second crystallization, which has the enthalpy of crystallization related to the exothermic DSC peak of ΔH_{P2} = 67.1 J/g, occurred above 825 K. The DSC curve of the cryogenically milled powder showed a 13 % decrease in ΔH_{P1} with a slight decrease in ΔH_{P2} (3 %), indicating the dominant precipitation of α-Fe(Si) by mechanical crystallization via a wear-like mechanism consisting of continuous bending, sliding, and rolling during the cryogenic milling.

XRD traces of the as-spun ribbon, as-milled samples, and fully crystallized ribbon are shown in Fig. 1(d). The result of the as-spun ribbon corresponds to that of amorphous $Fe_{78}Si_9B_{13}$, showing a halo pattern, whereas the XRD trace of the as-milled sample showed both the halo pattern and a peak of nanocrystalline α-Fe(Si). These results are consistent with those of Huang *et al.* [18], who milled $Fe_{78}Si_9B_{13}$ ribbons to produce nanocrystalline α-Fe and Fe_2B using cryogenic attritor milling. The absence of Fe_2B, which is identically thermally induced [18] herein, suggests that liquid nitrogen prevented a temperature rise during the pulverization of the $Fe_{78}Si_9B_{13}$ ribbons.

The effect of mechanical milling on the thermal stability of the Fe-based composite powders containing

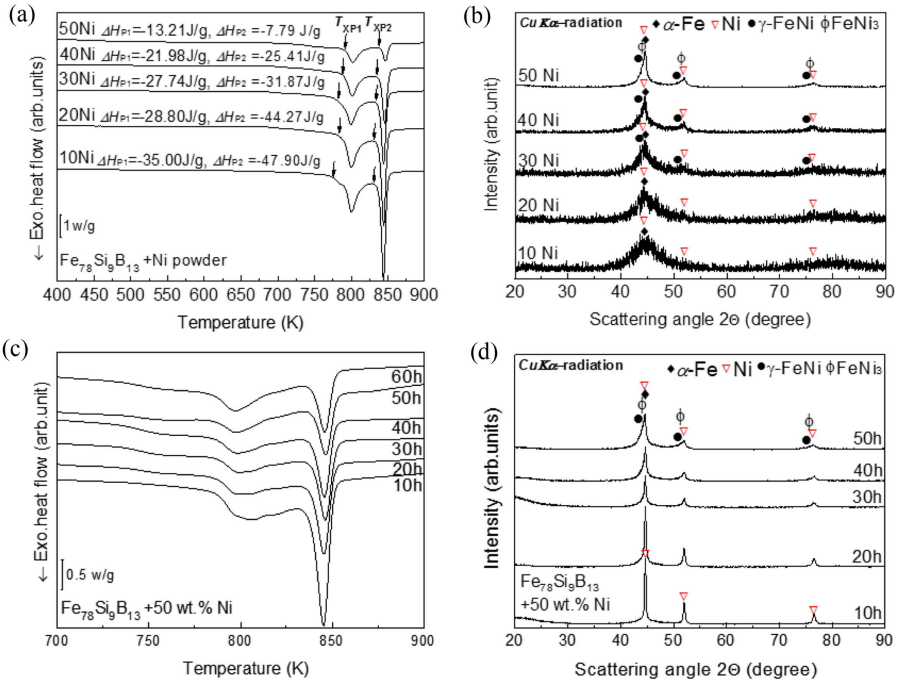

Fig. 2. (a) DSC curves (40 K/min) and (b) XRD patterns of Fe-based glassy composite (milled) powders containing 10, 20, 30, 40, and 50 wt.% Ni. (c) DSC and XRD patterns of 50 wt.% Ni composite powders with different milling durations.

10, 20, 30, 40, and 50 wt.% of Ni is shown in Fig. 2(a). The first crystallization temperature was affected by the Ni content and mechanical treatment. With an increase in the Ni content, the values of Tx_{P1} for the composite powders shifted to 790 K. Due to the mechanical crystallization by ball milling and the component ratio of amorphous and Ni particles, the crystallization enthalpy (the sum of ΔH_{P1} + ΔH_{P2}) of the composite powders decreased from about 82.9 (10 wt.% Ni composite powder) to 21.0 J/g (50 wt.% Ni composite powder). Considering the crystalline Ni weight fraction of the composites, the decrease by 16 % of crystallization enthalpy of 10, 20, 30, and 40 wt.% Ni composite powders represented the same mechanical crystallization after 50 h of mechanical alloying. However, the crystallization behavior of the 50 wt.% Ni milled composite was weird. The phase transformation of $FeNi_3$ synthesized by mechanical alloying to γ-FeNi showing endothermic reaction near at 882 K under the heating, resulted in the positive enthalpy, and the positive enthalpy summed the negative enthalpy of the exothermic second peak of the 50 wt.% Ni composite. As a result, it shows ~37 % reduction in total crystallization enthalpy and a drastically modified second exothermic peak compared with that of other as-milled composites. A similar phenomenon was obtained J.W. Christian [19] for the endothermic phase transformation of ordered $FeNi_3$ to disordered γ-FeNi at 882 K at a 40 K/min heating rate. Additionally, the XRD trace of the 50-h milled composite with 50 wt.% Ni confirmed the presence of $FeNi_3$ (Fig. 2(c) and (d)), indicating that endothermic reactions occurred only at 50 wt.% Ni composite under the heating condition.

XRD traces revealed peak broadening due to the mean inhomogeneous strain via mechanical treatment and Ni solid solution inhomogeneity of the as-milled powders containing up to 20 wt.% Ni (Fig. 2(b)). This indicates that self-diffusion and interdiffusion of nickel into the amorphous $Fe_{78}Si_9B_{13}$ matrix were induced by 50-h ball milling with continuous repetitive fracturing and cold welding since the free volume of an amorphous matrix plays an important role in the short-circuit diffusion paths [20]. A new Ni-containing amorphous alloy was formed due to the fast abnormal diffusion behavior of nickel atoms in the amorphous $Fe_{78}Si_9B_{13}$ alloy [21].

With an increase in Ni content higher than 20 wt.%, the intensity of the main peaks corresponding to the Ni and α-Fe phases increased and the shape became narrower and sharper. There were also traces of the formation of the γ-FeNi phase, indicated by the left-side widely asymmetric main peaks. When the nickel content was lower than 20 wt.%, nickel atoms entered completely into the amorphous matrix, and no evidence of diffusion of iron atoms from the amorphous matrix into the nickel matrix was observed. With Ni content above 20 wt.%, iron atoms from the amorphous phase, caused by decreasing the glass forming ability due to decreasing B/Si concentration ratio entered into the nickel-rich matrix, resulting in the production of the γ-FeNi phase [22]. This corresponds with the XRD results (Fig. 2(b)). Wang *et al.* [23] and Guittoum *et al*. [24] reported the occurrence of Ni solid solution in the amorphous phase or the formation of the γ-FeNi phase according to Ni contents, supporting the result obtained herein. The existence of $FeNi_3$ revealed by XRD in the milled 50 wt.% Ni composite (Fig. 2(d)) during 50-h mechanical alloying is attributed to the compositional characteristic of the 50 wt.% Ni composite. Table 1 shows the phase volume fraction of the as-milled composites with different Ni contents.

Figures 3(a)-(e) show the BSE micrographs of the cross-section for the milled composite powders with Fe-

Table 1. Quantitative phase volume fraction of 50-h as-milled composite powders containing 10, 20, 30, 40, and 50 wt.% Ni and the calculated and experimental saturation magnetization (M_s).

Composite powder / Phase (Ms)	Quantitative volume fraction (%)				
	10Ni	20Ni	30Ni	40Ni	50Ni
Fe-based glass (173 emu/g)	82.5	77.5	68.5	60.2	30.7
α-Fe (218 emu/g)	14.5	13.5	12.0	10.5	17.0
Ni (58 emu/g)	3 (Dissolution)	9 (Dissolution)	16	24	34
$Fe_{1.0}Ni_{1.0}$ (138 emu/g)			3.5	5.3	13.0
$Fe_{1.0}Ni_{3.0}$ (98 emu/g)					5.3
Sum (%)	100	100	100	100	100
Calculated Ms (emu/g)	176	166	155	143	127
Experimental Ms (emu/g)	180	171	158	146	130
Error (%)	2.2	3.0	2.0	2.3	2.0

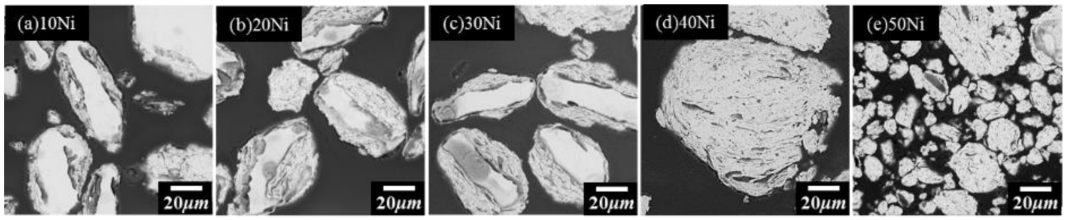

Fig. 3. BSE images of 10% Nital-etched cross-section of amorphous $Fe_{78}Si_9B_{13}$ matrix composite powders with (a) 10, (b) 20, (c) 30, (d) 40, and (e) 50 wt.% Ni.

based amorphous powder and various Ni contents. For low Ni-containing composites (Figs. 3(a)-(c)), the cross-sectional image of the as-milled particles appeared mainly in the microstructure consisting of Fe-based amorphous core surrounded by multilayers stacked repeatedly with Fe-amorphous alloy and Ni, whereas fine homogeneous layers were observed in small particles with ~ 10 um diameter (Fig. 3(a)). The microstructural features of the milled composites show that cold welding was predominant over powder fracturing during the milling process.

With an increase in the Ni content, the Fe-based glassy particles lost their original flake shape and were heavily deformed during mechanical milling. Furthermore, the layer gradually extended over the areas between the large and heavily deformed glassy particles.

Figures 4(a)-(c) show the EDS mapping images of the 10-, 30-, and 50-h milled composites containing 50 wt.% Ni. With an increase in milling duration, there was no boundary between Fe-based matrix and Ni additive, indicating the self-diffusion and interdiffusion of nickel into the Fe-amorphous powder. The microstructural features of the composites were also optimized considering the ratio of Fe matrix particle and Ni. Therefore, the cross-sectional features of the milled composite containing Ni 50 wt.% became more homogenous and fine in the entire particle without any amorphous core (Figs. 5(a)-(c)).

Figures 6(a) and (b) show the DSC curves and XRD patterns of the annealed Fe-based composite powders with 10, 20, 30, 40, and 50 wt.% Ni (at 673 K for 240 h). The quantitative phase analysis of these alloys was performed with a High Score Plus program using XRD traces. Table 2 lists the volume fraction of phases considering the residual amorphous phase in the annealed composite alloys.

The effect of heat treatment on the thermal stability of the as-annealed powders with 10, 20, 30, 40, and 50 wt.% Ni is shown in Fig. 6(a). As the precipitated Fe atoms from the amorphous matrix formed intermetallic compounds

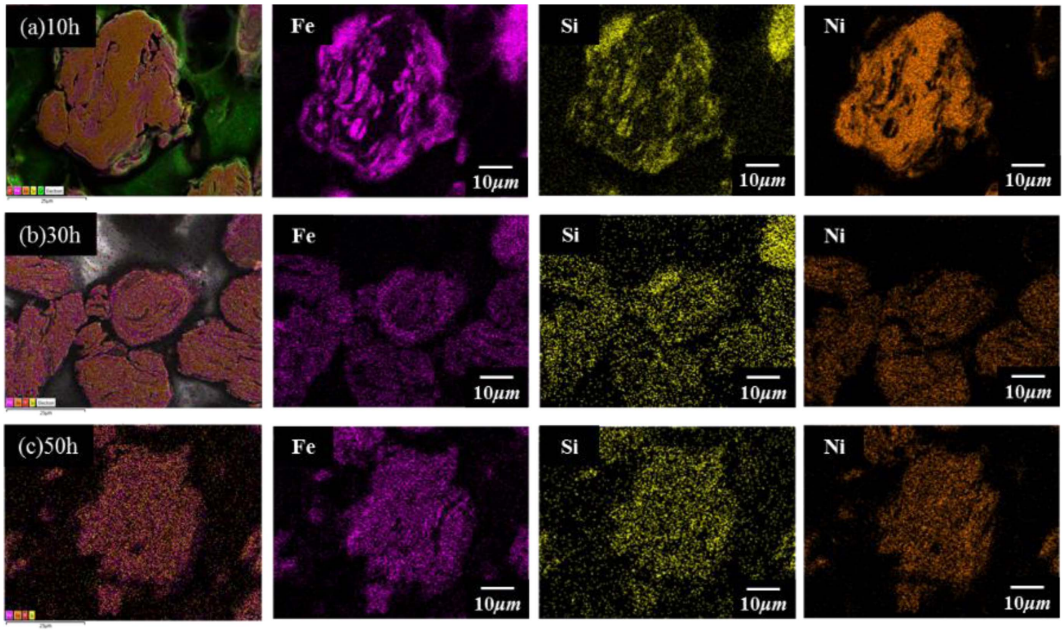

Fig. 4. (Color online) EDS elemental mapping of the polished cross-section of the Fe-based composite powder containing 50 wt.% Ni mechanically milled for (a) 10, (b) 30, and (c) 50 h (Fe indexed by purple, Si indexed by yellow, and Ni indexed by orange).

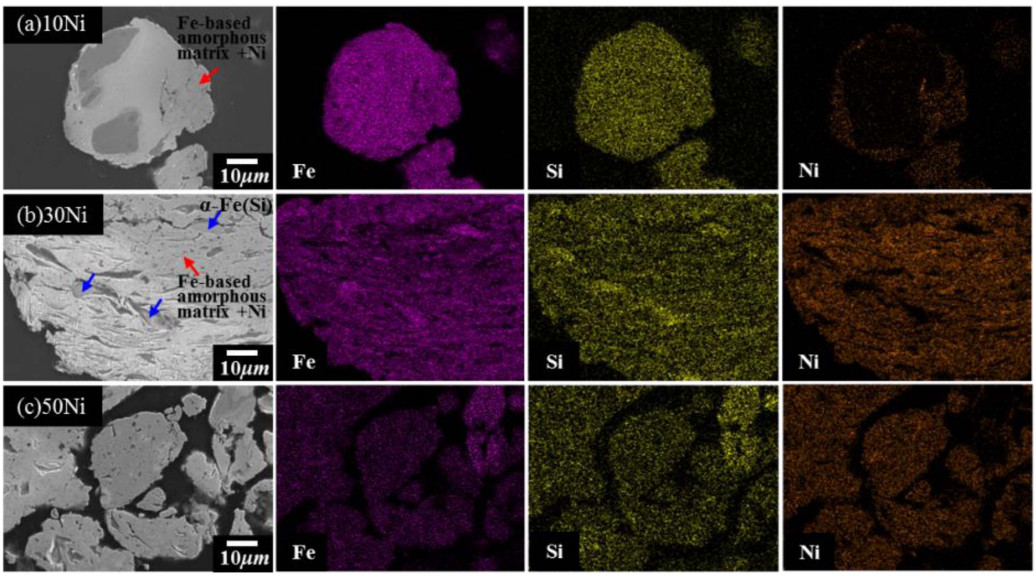

Fig. 5. (Color online) EDS elemental mapping of the polished cross-section of Fe-based composite powders with (a) 10, (b) 30, and (c) 50 wt.% of Ni (Fe indexed by purple, Si indexed by yellow, and Ni indexed by orange).

with Ni, the chemical composition of the Fe-based amorphous matrix with relatively high concentration of boron as a metalloid and residual dissolved Ni was modified, resulting in a single exothermic peak with a slight shift to a higher temperature. This is similar to the thermal stability feature of the amorphous Fe–Si–B matrix. Gibson [25] reported that only a single exothermic peak is observed for high boron content in amorphous Fe–Si–B alloys, and this agrees well with Fig. 6(a).

For the annealed composite with 10 wt.% Ni, some diffraction peaks ascribed to α-Fe and BCC $Fe_{0.7}Ni_{0.3}$ were observed in the XRD pattern (Fig. 6(b)). As the Ni content increased above 10 wt.%, the peak intensity of the BCC α-(Fe,Ni) alloys decreased due to the partial structural phase transition from BCC α-(Fe,Ni) to FCC γ-(Fe,Ni). However, the peak intensity of the FCC γ-(Fe,Ni) phase increased. The α-(Fe,Ni) phase in the annealed composites maintained either $Fe_{0.7}Ni_{0.3}$ or $Fe_{1.2}Ni_{0.8}$. Ni, which has a higher diffusion coefficient than that of Fe [26], diffused into the primary precipitated α-Fe (BCC) at 673 K, forming BCC α-(Fe,Ni) compounds. In the case of the FCC-(Fe,Ni) phases, the quantitative fractions of the FCC-(Fe,Ni) phases, such as γ-FeNi and γ'-$FeNi_3$ (up to 48 vol.%), were enlarged due to the partial phase transformation of BCC-(Fe,Ni) to FCC-(Fe,Ni), the formation of new γ-FeNi induced from Ni-rich region, and the decomposition of γ-FeNi to α-Fe and γ'-$FeNi_3$. With an increase in the Ni content, the BCC-(Fe,Ni) phases transformed into FCC-(Fe,Ni), which is a thermodynamic stable phase with lower Gibbs free energy than that of

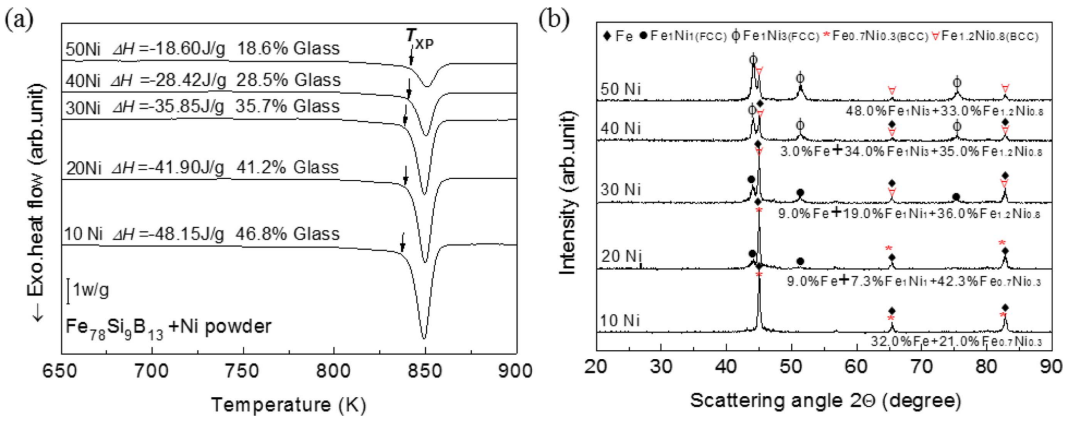

Fig. 6. (Color online) (a) DSC curves (40 K/min) and (b) XRD patterns of annealed Fe glassy/Ni composite (milled) powders with 10, 20, 30, 40, and 50 wt.% Ni at 673 K for 240 h.

Table 2. Quantitative phase volume fraction of annealed composite powders containing 10, 20, 30, 40, and 50 wt.% Ni (at 673 K for 240 h) and the calculated and experimental M_s.

Phase (Ms) \ Composite powder	Quantitative volume fraction (%)				
	10Ni	20Ni	30Ni	40Ni	50Ni
FeNi-based glass (153 emu/g)	46.8	41.2	35.7	28.5	18.6
α-Fe (218 emu/g)	32.0	9.0	9.0	3.0	
$Fe_{0.7}Ni_{0.3}$ (171 emu/g)	21.0	42.3			
$Fe_{1.2}Ni_{0.8}$ (154 emu/g)			36.0	35.0	33.0
$Fe_{1.0}Ni_{1.0}$ (138 emu/g)		7.3	19.0		
$Fe_{1.0}Ni_{3.0}$ (98 emu/g)				34.0	48.0
Sum (%)	100	100	100	100	100
Calculated Ms (emu/g)	177.2	165.0	156.0	137.4	126.4
Experimental Ms (emu/g)	176.2	166.0	155.2	136.5	127.8
Error (%)	0.6	0.6	0.5	0.7	1.2

BCC -(Fe,Ni) [15]. This transformation behavior agrees with that reported by Jiraskova *et al.* [27, 28].

In terms of the decomposition of chemically-disordered γ-(Fe, Ni), it might be considered an eutectoid reaction of γ-(Fe, Ni) with to α-Fe and chemically-ordered γ'-$FeNi_3$ during the heat treatment. The formation of new γ-FeNi from the Ni-rich region is a well-known phase transition, and a similar trend was reported by Liu *et al.* [29].

During annealing, amorphous phases undergo structural relaxation, phase separation, and crystallization, resulting in their active diffusion behavior according to their chemical constituents and the annealing temperature [30]. For example, structural relaxation normally can occur at temperatures below T_g, and phase separation in the glassy alloy occurs at temperatures around T_g (either below, at, or above T_g). These processes involve atomic diffusion, accompanied by phase transformation. Therefore, the annealing temperature of amorphous precursors for $L1_0$ FeNi should be between the glass-transition temperature and the crystallization-onset temperature. Considering the crystallization temperature of the as-milled composite powders, annealing can be performed at about 789 K. However, recent experimental studies on NWA 6259 meteorites by temperature-dependent magnetization measurements using VSM have shown that the degradation of the saturation magnetization (M_s) and coercivity (H_c) starts at about 803 K due to the disordering of $L1_0$ FeNi phase. Hence, the annealing temperature of 673 K, which is lower than the crystallization- onset temperature (789 K) of the amorphous Fe–Si–B system needs the boosting of the diffusivity of defects formed by mechanical treatment, such as mechanical milling and alloying, and unusually long annealing for glass crystallization after phase relaxation. In addition, the large temperature difference between the crystallization-onset and heat-treatment temperatures of the composite powder was inadequate for $L1_0$ formation, despite the milling-induced defects.

The magnetic properties of the as-milled precursors and as-annealed composite powders were investigated at room temperature using a VSM. Figs. 7(a) and 8(a) depict the magnetization (M–H) loops of the as-milled precursors and annealed powders with varying Ni contents, respec-

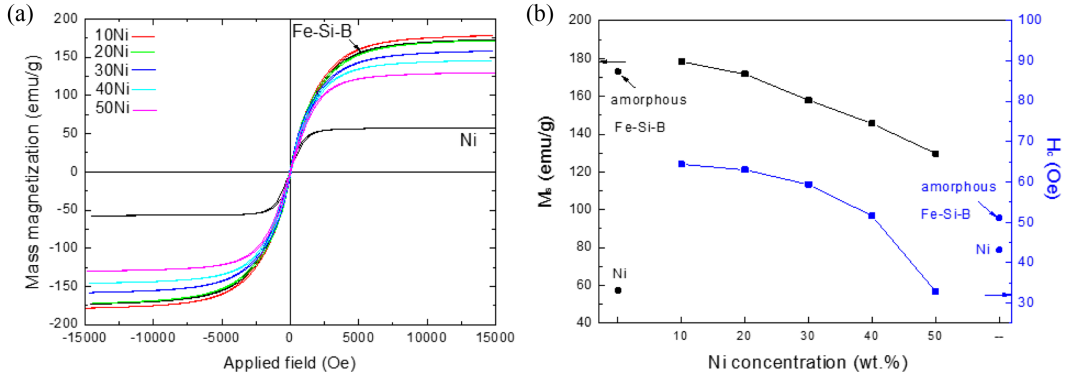

Fig. 7. (Color online) M–H hysteresis loops of (a) 50-h as-milled composite powders with 10, 20, 30, 40, and 50 wt.% Ni measured at 300 K. (b) composition-dependent M_s and H_c of as-milled composite powders.

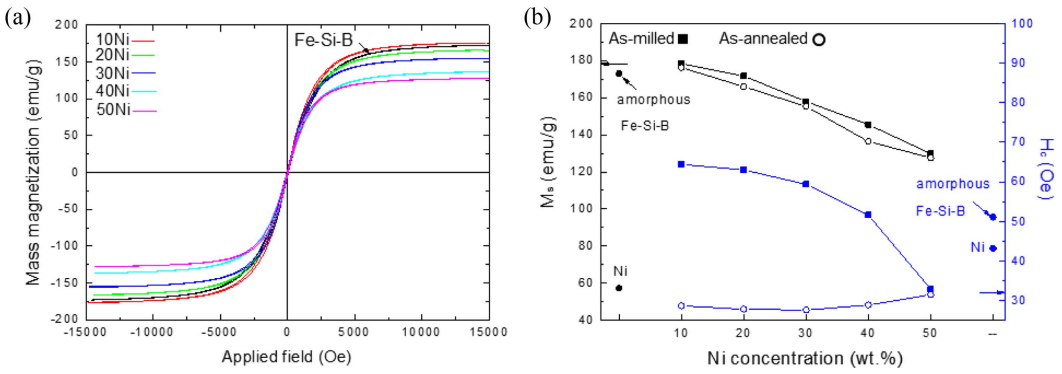

Fig. 8. (Color online) M–H hysteresis loops of (a) annealed composite powders with 10, 20, 30, 40, and 50 wt.% Ni (at 673 K for 240 h) measured at 300 K. (b) Composition-dependent M_s and H_c of annealed composite powders.

tively. The loops show a typical magnetization behavior for soft magnetic materials. Figs. 7(b) and 8(b) show M_s and H_c according to the Ni contents taken from the M–H loops (Figs. 7(a) and 8(a)) to compare the effect of Ni contents and annealing on the magnetic behavior. The M_s and H_c of the amorphous $Fe_{78}Si_9B_{13}$ and Ni powders were 173 and 58 emu/g with 51 and 43 Oe, respectively (Fig. 7(b)).

Table 1 shows the variation in the saturation magnetization values of the as-milled precursors. The values decreased from 180 to 130 emu/g as the Ni content increased, and they agree well with the calculated values for varying volume fractions of the amorphous matrix, Ni additive, α-Fe, γ-FeNi, and γ'-$FeNi_3$ analyzed by DSC, XRD, and ICP.

The coercive force of amorphous materials is lower than that of crystalline materials due to the compensation of magnetic anisotropic force caused by the short-range ordered atomic structure. In this study, however, as-milled powders showed relatively high coercivity, except that containing 50 wt.% Ni, due to the increase in the defect density and internal stress during mechanical milling. Defects, such as dislocations or grain boundaries, accompanied by internal stress during mechanical milling act as pinning sites, obstructing domain wall displacement. Thus, the coercivity increases due to the reduced magnetic response from the magnetic field. The coercive force of the as-milled composites with above 30 wt.% Ni contents showed a decreasing tendency, and it is attributed to both the formation of α-Fe and γ-FeNi and the increase in the phase fraction.

After annealing, the M_s values were similar to a slight difference of ~4.7 emu/g as a mean value compared with that of the as-milled precursors, and the coercivity varied among the newly formed FeNi compounds, as shown in Fig. 8(b).

The magnetic moments of standard crystalline Fe and Ni per cell are about 2.2 and 0.6 μB, respectively [31], and their M_s are 218 and 57 emu/g, respectively, as determined by VSM measurement. Therefore, the bulk M_s of $Fe_{1-X}Ni_X$ is estimated to be 218 (1–X) + 58 X (emu/g).

Additionally, the standard M_s of Fe-based amorphous alloys (173 emu/g) was reset to a value for FeNi-based amorphous alloys (about 153 emu/g) [32] due to the precipitation of α-Fe(Si). Herein, the experimental M_s of the annealed composites was very close to the estimated bulk value due to the phase fraction of the annealed composite powders, corresponding to the XRD and DSC results. Table 2 shows the phase volume fraction and the evaluation of experimental and calculated magnetization of the as-annealed composites.

The coercive force of the heat-treated composites decreased due to the relieving of internal stress, which serves as pinning sites, when the excess free volume of the amorphous matrix was eliminated by rearrangement via diffusion during low-temperature heat treatment than crystallization temperature to make perfect short-range atomic order. Furthermore, the decrease in coercive force after heat treatment is attributed to the formation of FeNi compounds having lower magneto-crystalline anisotropy.

However, the result shows a tendency to increase the coercivity of the annealed composites containing more than 30 wt.% Ni due to the formation of $FeNi_3$ compounds having high absolute values of negative magneto-crystalline anisotropy. As the milled composites were annealed, phase transformation of γ-FeNi to thermodynamically stable α-Fe and $FeNi_3$ occurred, and the fraction of $FeNi_3$ also increased. However, α-Fe and Ni formed new BCC-(Fe,Ni) compounds, such $Fe_{1.2}Ni_{0.8}$, after the phase transformation.

The presence of the $L1_0$ phase was not confirmed at any stage of our investigation, whereas the magnetic behavior of the annealed composites indicates the formation of α-Fe, γ-FeNi, and $Fe_{1-X}Ni_X$ in the Fe-amorphous matrix,

depending on the Ni content. However, the Fe-based amorphous composites comprising Fe–Ni alloy are considerable soft magnetic materials owing to improved coercivity compared to that of the as-milled $Fe_{78}Si_9B_{13}$, which is contrary to the initial expectations.

4. Conclusions

In this study, we synthesized FeNi-based composites via high-energy ball milling for the preparation of high-internal-energy precursors consisting of a Fe-based amorphous matrix. Mechanical alloying was employed to produce amorphous $Fe_{78}Si_9B_{13}$ composite powders containing 10, 20, 30, 40, and 50 wt.% Ni. The microstructures of the milled composites were dependent on the Ni content. SEM images of composites with high Ni content showed fully multilayered structures, whereas the of the composites with low Ni contents revealed Fe-based amorphous core surrounded by alternating layers of Fe-based amorphous alloy and Ni.

With Ni content lower than 20 wt.%, nickel atoms completely diffused into the amorphous matrix, and no evidence of diffusion of atoms from the amorphous matrix into the nickel matrix was observed. As the Ni content increased above 20 wt.%, iron atoms from the amorphous phase could diffuse into the Ni-rich matrix, producing γ-FeNi and γ'-$FeNi_3$ phases.

After annealing the milled composite powders at 673 K for 240 h, all annealed samples formed a complex of the amorphous matrix containing either α-Fe and BCC-(Fe, Ni) or α-Fe, BCC-(Fe, Ni), and FCC-(Fe, Ni).

The Fe-based amorphous composites comprising the (Fe,Ni) compound exhibited higher saturation magnetization than that of the cryo-milled $Fe_{78}Si_9B_{13}$ with improved coercivity than a single component, indicating that the composite is a soft magnetic material.

The phase transformation of the annealed composites at 673 K resulted in relatively dominant atomic diffusion of Ni over Fe and increased diffusivity as a function of Ni content. However, the annealing temperature (673 K) was lower than the crystallization-onset temperature (789 K) of the amorphous Fe–Si–B system; thus, unusually long annealing was required to achieve glass crystallization after phase relaxation. The formation of the $L1_0$ phase was not confirmed at any stage of our study. There is a need, therefore, for further investigation of the ordered–disordered transition temperature of $L1_0$ FeNi in the range of 673–823 K. Although we could not successfully synthesize artificial $L1_0$ FeNi alloys, this study would serve as a valuable reference for further studies on artificial $L1_0$ FeNi alloys.

Acknowledgment

This research was supported by the Basic Science Research Program through the National Research Foundation of Korea (NRF) funded by the Ministry of Education (2017R1A 6A3A01011500).

References

[1] S. Vittaa, A. Khuntiaa, G. Ravikumarb, and D. Bahadura, J. Magn. Magn. Mater. **320**, 182 (2008).
[2] M. M. Abd-Elmeguid, B. Schleede, and H. Micklitz, J. Magn. Magn. Mater. **72**, 253 (1988).
[3] T. Shima, M. Okamura, S. Mitani, and K. Takanashi, J. Magn. Magn. Mater. **310**, 2213 (2007).
[4] M. Mizuguchi, S. Sekiya, and K. Takanashi, J. Appl. Phys. **107**, 09A716 (2010).
[5] M. Mizuguchi, T. Kojima, M. Kotsugi, T. Koganezawa, K. Osaka, and K. Takanashi, J. Magn. Soc. Jpn. **35**, 370 (2011).
[6] T. Kojima, M. Mizuguchi, and K. Takanashi, J. Phys.: Conf. Ser. **266**, 012119 (2011).
[7] J. Albertsen, J. Knudsen, and G. Jensen, Nature **273**, 453 (1978).
[8] R. S. Clarke and E. R. Scott, Am. Mineral. **65**, 624 (1980).
[9] J. Albertsen, Phys. Scr. **23**, 301 (1981).
[10] L. Néel, J. Pauleve, R. Pauthenet, J. Laugier, and D. Dautreppe, J. Appl. Phys. **35**, 873 (1964).
[11] T. Nagata and M. Funaki, Mem. Nat. Inst. Polar Res. **46**, 245 (1987).
[12] V. F. Buchwald, Handbook of iron meteorites: their history, distribution, composition and structure, University of California, Berkeley (1975).
[13] M. Kotsugi, C. Mitsumata, H. Maruyama, T. Wakita, T. Taniuchi, K. Ono, M. Suzuki, N. Kawamura, N. Ishimatsu, M. Oshima, Y. Watanabe, and M. Taniguchi, Appl Phys Express. **3**, 013001 (2009).
[14] T. Kojima, M. Mizuguchi, T. Koganezawa, K. Osaka, M. Kotsugi, and K. Takanashi, Jpn. J. Appl. Phys. **51**, 010204 (2012).
[15] A. Makino, P. Sharma, K. Sato, A. Takeuchi, Y. Zhang, and K. Takenaka, Sci. Rep. **5**, 16627 (2015).
[16] Y. Geng, T. Ablekim, M. A. Koten, M. Weber, K. Lynn, and J. E. Shield, J. Alloys Compd. **633**, 250 (2015).
[17] G. S. Was, Fundamentals of Radiation Materials Science, Springer, New York (2007).
[18] B. Huang, H. G. Jiang, R. J. Perez, S. R. Nutt, and E. J. Lavernia, Nanostruct. Mater. **11**, 1009 (1999).
[19] J. W. Christian, The theory of transformations in metals and alloys, Pergamon, United Kingdom (1975).
[20] M. X. Quan, K. Y. Wang, T. D. Shen, and J. T. Wang, J. Alloys Compd. **194**, 325 (1993).
[21] B. S. Bokstain, L. M. Klinger, I. M. Razumovski, and E. N. Uvarova, Fiz. Met. Metalloved. **51**, 561 (1981).

[22] R. Ray, R. Hasegawa, C. P. Chou, and L. A. Davis, Scr. Metall. **11**, 973 (1977).
[23] K. Y. Wang, J. T. Wang, M. X. Quan, and W. D. Wei. Mater. Sci. Forum **88-90**, 283 (1992).
[24] A. Guittoum, A. Layadi, A. Bourzami, H. Tafat, N. Souami, S. Boutarfaia, and D. Lacour, J. Magn. Magn. Mater. **320**, 1385 (2008).
[25] M. A. Gibson, Ph.D. Thesis, University of Wollongong, Australia (1988).
[26] K. Arioka, Y. Iijima, and T. Miyamoto, Philos. Mag. **95**, 3577 (2015).
[27] Y. Jiraskova, J. Bursik, I. Turek, M. Hapla, A. Titov, and O. Zivotsky, J. Alloys Compd. **594**, 133 (2014).
[28] H. Bakker, H. P. Bonzel, C. M. Bruff, M. A. Dayananda, W. Gust, J. Horváth, I. Kaur, G. V. Kidson, A. D. LeClaire, H. Mehrer, G. E. Murch, G. Neumann, N. Stolica, and N. A. Stolwijk, Diffusion in Solid metals and alloys, Springer, Berlin (1990).
[29] J. Liu, L. J. Riddiford, C. Floristean, F. Goncalves-Neto, M. Rezaeeyazdi, L. H. Lewis, and K. Barmak, J. Alloys Compd. **689**, 593 (2016).
[30] C. Suryanarayana, A. Inoue, Bulk metallic glasses, CRC, United States (2011).
[31] L. J. Swartzendruber, V. P. Itkin, and C. B. Alcock, The Fe-Ni (iron-nickel) system, J. Phase Equilib. **12**, 288 (1991).
[32] F. Luborsky, J. Becker, J. Walter, and H. Liebermann, IEEE Trans. Magn. **15**, 1146 (1979).